UDC 621.316 https://doi.org/10.20998/2074-272X.2026.2.04

S. Belakehal, M.L. Srief

Comparative performance analysis of backstepping and sliding mode control for static synchronous compensators based on flying capacitor multicell converters

Introduction. *The integration of a static synchronous compensator (STATCOM) based on a flying capacitor multicell converter (FCMC) provides an effective solution for dynamic reactive power compensation and voltage quality improvement. The adoption of nonlinear control strategies, such as sliding mode control (SMC) and backstepping (BSC), enhances system robustness and ensures precise tracking of variables despite network nonlinearities and disturbances.* ***Problem.*** *Reactive, inductive or capacitive loads cause network imbalances leading to voltage sags, swells and fluctuations at the point of common coupling (PCC). These disturbances degrade power quality, reduce the power factor and place excessive stress on equipment. Moreover, high reactive power flow increases losses and decreases the overall system efficiency.* ***Goal.*** *This study compares the performance of SMC and BSC controllers applied to a STATCOM for PCC voltage regulation aiming to improve the power factor, effectively control reactive power and overcome the limitations of conventional controllers under network nonlinearities and voltage disturbances caused by reactive loads.* ***Methodology.*** *The SMC uses a sliding surface based on current errors to achieve fast and precise tracking even in the presence of disturbances. The BSC control employs Lyapunov functions to decompose the nonlinear system into controllable subsystems, ensuring overall stability. Both strategies are simulated on a 5-level flying capacitor multicell STATCOM using MATLAB/Simulink. Simulation* ***results*** *confirm the effectiveness of both controllers in maintaining the PCC voltage at its reference value with a very short response time (1 ms), even under reactive load variations. Precise reactive power control enables rapid compensation of fluctuations, improves the power factor and reduces harmonic distortion. The* ***scientific novelty*** *of this work lies in the comparative performance analysis of the nonlinear SMC and BSC controllers applied to a STATCOM based on a FCMC converter, considering network disturbances caused by reactive loads.* ***Practical value.*** *These nonlinear control strategies significantly enhance the stability, voltage quality, and power factor of low-voltage networks equipped with STATCOMs.* References 36, tables 4, figures 18.

Key words: **flying capacitor multicell converter, static synchronous compensator, sliding mode control, PI controller.**

Вступ. *Інтеграція статичного синхронного компенсатора (STATCOM) на основі багатоелементного перетворювача з літаючим конденсатором (FCMC) забезпечує ефективне рішення для динамічної компенсації реактивної потужності та покращення якості напруги. Впровадження нелінійних стратегій керування, таких як ковзне керування (SMC) та зворотний крок (BSC), підвищує стійкість системи та забезпечує точне відстеження змінних, незважаючи на нелінійність та збурення мережі.* ***Проблема***. *Реактивні, індуктивні або ємнісні навантаження викликають дисбаланс мережі, що призводить до знижень, збільшень та коливань напруги в точці спільного підключення (PCC). Ці збурення погіршують якість електроенергії, знижують коефіцієнт потужності та створюють надмірне навантаження на обладнання. Крім того, високий потік реактивної потужності збільшує втрати та знижує загальну ефективність системи.* ***Мета***. *У цьому дослідженні порівнюється продуктивність контролерів SMC та BSC, що застосовуються до STATCOM для регулювання напруги PCC, з метою покращення коефіцієнта потужності, ефективного керування реактивною потужністю та подолання обмежень традиційних контролерів за умов нелінійності мережі та збурень напруги, спричинених реактивними навантаженнями.* ***Методика***. *SMC використовує ковзну поверхню на основі похибок струму для досягнення швидкого та точного відстеження навіть за наявності збурень. Керування BSC використовує функції Ляпунова для розкладання нелінійної системи на керовані підсистеми, забезпечуючи загальну стабільність. Обидві стратегії моделюються на п'ятирівневому багатоелементному STATCOM з літаючим конденсатором за допомогою MATLAB/Simulink.* ***Результати*** *моделювання підтверджують ефективність обох контролерів у підтримці напруги PCC на її опорному значенні з дуже коротким часом відгуку (1 мс), навіть за коливань реактивного навантаження. Точне керування реактивною потужністю дозволяє швидко компенсувати коливання, покращує коефіцієнт потужності та зменшує гармонійні спотворення.* ***Наукова новизна*** *роботи полягає в порівняльному аналізі продуктивності нелінійних контролерів SMC та BSC, застосованих до STATCOM на основі перетворювача FCMC, з урахуванням мережевих збурень, спричинених реактивними навантаженнями.* ***Практична значимість***. *Ці нелінійні стратегії керування значно покращують стабільність, якість напруги та коефіцієнт потужності низьковольтних мереж, оснащених STATCOM.* Бібл. 36, табл. 4, рис. 18.

Ключові слова: **багатоелементний перетворювач з літаючим конденсатором, статичний синхронний компенсатор, керування ковзним режимом, ПІ-регулятор.**

Introduction. Flexible AC transmission systems (FACTS) have been widely adopted in modern power networks to enable efficient control of power flow, enhance the maximum transferable power, regulate voltage profiles, improve power factor, and strengthen overall system stability. In addition, certain FACTS devices contribute to network frequency management, thereby supporting reliable and flexible operation of the electrical grid [1, 2]. Within the wide range of FACTS devices, the static synchronous compensator (STATCOM) has received considerable attention due to its robustness and capability to provide dynamic reactive power with rapid response [3]. It is widely regarded as one of the most effective FACTS devices. When connected in parallel with the power grid, the STATCOM operates via voltage source converters integrated into the transmission network. Its operating principle relies on controlling the reactive power exchanged between the converter and the grid, analogous to the behavior of a rotating synchronous machine [4, 5]. This exchange is accomplished through 3-phase voltages of adjustable amplitude and frequency, which are synchronized with the grid and generated from a DC voltage source maintained by charged capacitors [6].

The implementation of a STATCOM can be achieved using a conventional 2-level voltage source converter, as reported in earlier studies [5]. Such converters offer several advantages, including a reduced component count, the use of at most two DC voltage sources, and relatively straightforward control strategies. However, they exhibit significant limitations, such as poor output voltage quality, high harmonic distortion, and applicability restricted to low-voltage and low-to medium-power systems. In recent years, 2-level converter-based STATCOMs have increasingly been supplanted by multilevel converter technologies. Multilevel converters provide numerous benefits, including an increased number of output voltage levels, superior harmonic performance, higher efficiency,

improved power quality, reduced total converter losses, and lower electromagnetic interference due to decreased d*v*/d*t* stresses in the system [7–9]. Accordingly, considerable research efforts are currently directed toward the design, optimization and control of STATCOM topologies based on multilevel converters.

As demonstrated in several studies [7–12], 3 main multilevel converter structures are commonly identified:

1) cascaded H-bridge converters;
2) neutral-point clamped converters;
3) flying capacitor multicell converters (FCMCs).

The FCMC offers several compelling advantages for medium voltage applications. Notably, it can operate without a transformer, requires no clamping diodes, and inherently maintains its floating-capacitor voltages at their nominal values. This natural self-balancing property enables the design of converters with a large number of voltage levels [13, 14].

However, one of the main control challenges in FCMCs lies in maintaining stable and balanced voltages across all floating capacitors. In the absence of an effective balancing mechanism, the voltages of these capacitors can drift from their nominal values, thereby increasing the electrical stress on the power switches. To ensure reliable voltage balancing, these structures generally rely on advanced modulation techniques, notably phase-shifted pulse width modulation (PS-PWM) [15, 16].

The interleaved carrier modulation technique, widely known as PS-PWM, is the conventional control strategy employed in flying-capacitor converters. This method is particularly effective because the phase-shifted switching patterns naturally distribute the charge among the floating capacitors, thereby maintaining their voltage balance without requiring additional control loops. By preserving the inherent self-balancing property of the capacitor voltages, PS-PWM ensures reliable operation of the switching devices and enhances the overall stability of the converter [17, 18].

Recent research efforts have been directed towards enhancing the performance of multilevel STATCOM systems through PWM-based control approaches. In [19], the authors studied a 5-level half-bridge modular multilevel converter (MMC) for D-STATCOM applications, employing phase disposition modulation and a PI controller to effectively balance the capacitor voltages. The authors in [20] proposed a flexible modeling approach for a delta-connected MMC STATCOM with embedded energy storage, aiming to optimize reactive power compensation and system interface control. Finally, the authors of [21] developed a variable DC voltage control strategy for MMC-STATCOMs, which improves the reactive power response and stabilizes capacitor voltages under various operating conditions.

The goal of the work. This study compares the performance of sliding mode control (SMC) and backstepping (BSC) controllers applied to a STATCOM for point of common coupling (PCC) voltage regulation aiming to improve the power factor, effectively control reactive power and overcome the limitations of conventional controllers under network nonlinearities and voltage disturbances caused by reactive loads. The BSC provides stable and precise regulation of voltage and reactive current, while the SMC offers high robustness and a fast dynamic response, with a minor chattering effect. Both methods outperform linear controllers such as PID and linear quadratic regulator in STATCOM applications by effectively handling nonlinearities and network disturbances, while enabling precise balancing of floating capacitors and optimization of reactive power flow, thereby ensuring improved overall stability and performance.

System under study. The studied system (Fig. 1) consists of a 3-phase voltage source and 2 types of balanced 3 phase loads: a fixed active load and 2 dynamic reactive loads. The setup also includes a multilevel STATCOM comprising a DC energy source typically provided by high-capacity capacitors coupled with a 5-level FCMC. The compensator is connected to the PCC through a 3-phase filter inductor, enabling effective voltage regulation and mitigation of network disturbances. The control subsystem, which includes the reference signal generator and the controller, ensures dynamic voltage regulation while maintaining the desired power factor. The exchange of reactive power between the grid and the STATCOM is controlled by adjusting the compensator's output voltage V_c.

When the STATCOM voltage exceeds the grid voltage at the point of PCC, reactive power is injected into the grid. Conversely, if the grid voltage is higher than the STATCOM voltage, reactive power flows from the grid to the compensator. When the two voltages are equal, there is no exchange of reactive power [22, 23].

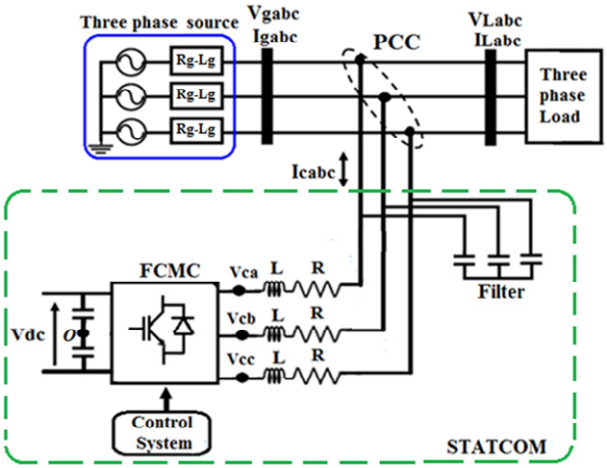

Fig. 1. Equivalent circuit of STATCOM

Mathematical modeling of the STATCOM. The circuit of a distribution system controlled by a STATCOM is shown in Fig. 1. In this system, V_{gabc} denote the 3-phase grid voltages at the PCC, V_{cabc} represent the 3-phase output voltages of the converter, and I_{cabc} are the corresponding STATCOM output currents. Moreover, L denotes the coupling filter inductance per phase, while R represents the series resistance, which accounts for both the winding resistance of the coupling filter and the conduction losses of the converter.

The instantaneous phase voltages at the PCC are:

$$V_{ga} = V_m \cos \omega t \; ; \tag{1}$$

$$V_{gb} = V_m \cos(\omega t - 2\pi/3) \; ; \tag{2}$$

$$V_{sc} = V_m \cos(\omega t - 4\pi/3) \; . \tag{3}$$

According to Kirchhoff's law of voltages, the relationship between the voltage at the PCC, the converter output voltage and the currents is as follows [24–26]:

$$V_{gabc} = V_{cabc} + RI_{cabc} + L\frac{\mathrm{d}I_{cabc}}{\mathrm{d}t} \; . \tag{4}$$

Using the Park transformation (*abc-dq*), the equation (4) can be rewritten as follows:

$$V_d = V_{cd} + RI_d + L\frac{\mathrm{d}I_d}{\mathrm{d}t} - L\omega I_q ; \quad (5)$$

$$V_q = V_{cq} + RI_q + L\frac{\mathrm{d}I_q}{\mathrm{d}t} + L\omega I_d , \quad (6)$$

where I_d, I_q are the d and q axis currents corresponding to I_{ca}, I_{cb}, I_{cc}; ω is the synchronized angular velocity of rotation of the voltage vector; V_{cd}, V_{cq} are the d and q axis voltages corresponding to V_{ca}, V_{cb}, V_{cc}.

According to the theory of instantaneous power, the active and reactive power exchanged between the network and the STATCOM can be calculated in the dq frame as:

$$P = \frac{3}{2}(V_d I_d + V_q I_q) ; \quad (7)$$

$$Q = \frac{3}{2}(V_q I_d - V_d I_q) . \quad (8)$$

In the synchronized rotary reference frame $V_g = V_d$ and $V_q = 0$, the instantaneous active and reactive powers can be written as follows:

$$P = \frac{3}{2}V_d I_d ; \quad (9)$$

$$Q = -\frac{3}{2}V_d I_q . \quad (10)$$

FCMC model. FCMC is based on the series connection of multiple switching cells, which allows the generation of high voltages with low harmonic distortion. Each phase of the converter consists of a set of p cells, interleaved with (p–1) floating capacitors. Each cell comprises 2 bidirectional switches (IGBTs), operated complementarily to prevent short circuits between voltage sources [16, 27, 28]. The binary state S_{ki} of switching cell (i =1, 2, 3,..., p) in phase (k = a, b, c) corresponds to the state of the upper switch of the cell: S_{ki} = 1 when the switch is closed, and S_{ki} = 0 when it is open.

The converter output voltage V_{kO} can then be expressed as a function of the switching states S_{ki} according to the following relationship:

$$V_{kO} = \frac{V_{dc}}{p}\left(\sum_{i=1}^{p} S_{ki} - p/2\right). \quad (11)$$

In a state of equilibrium, the voltages of the cells are equal:

$$V_{Ccellki} = V_{dc} / p . \quad (12)$$

Under these conditions, the voltages of the capacitors are given by:

$$V_{Cki} = \frac{i \cdot V_{dc}}{p} . \quad (13)$$

For a converter with p cells, the number of levels that the converter is capable of generating at the output is p+1. The characteristic values per phase of the combination of p switching cells are defined in Table 1.

Table 1

Definition of the per phase characteristic parameters of FCMC

Number of cells	p
Number of active switches	$2p$
Number of flying capacitors	p–1
Number of combinations	2^p
Number of generated output voltage levels	p+1
Main supply voltage value	V_{dc}
Voltage source of each cell i	$i \cdot V_{dc} / p$

In the specific case where the converter consists of 4 cells, it is referred to as a 5-level series multicell converter. Figure 2 illustrates the structure of one arm of this converter, which is composed of 8 switches forming 4 switching cells connected in series, along with 3 floating capacitors. The DC bus, in turn, consists of 2 capacitors, denoted C1 and C2.

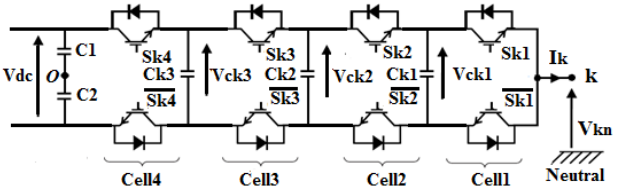

Fig. 2. Per-leg circuit configurations of the 5-level FCMC

The output voltages of the converter, measured with respect to the negative terminal O of the DC bus, are expressed as follows [29]:

$$V_{kO} = (S_{k4} - 0.5)\cdot V_{dc} + (S_{k3} - S_{k4})\cdot V_{ck3} + (S_{k2} - S_{k3})\cdot V_{ck2} + (S_{k1} - S_{k2})\cdot V_{ck1}. \quad (14)$$

The switches states of 4-cell 5-level FCM converter are demonstrated in Table 2.

Table 2

States of switches in the 4-cell-5-level FCMC

Output voltage level	States of (S_{k1}, S_{k2}, S_{k3}, S_{k4})	Number of state
V_{dc}/2	(1, 1, 1, 1)	1
V_{dc}/4	(1, 1, 1, 0) (1, 1, 1, 1) (1, 1, 0, 1) (0, 1, 1, 1)	4
0	(1, 1, 0, 0) (1, 0, 0, 1) (0, 0, 1, 1) (0, 1, 1, 0)	4
–V_{dc}/4	(0, 0, 0, 1) (0, 0, 1, 0) (0, 1, 0, 0) (1, 0, 0, 0)	4
–V_{dc}/2	(0, 0, 0, 0)	1

For a balanced 3-phase system, the sum of the 3 phase voltages is zero:

$$V_{an} + V_{bn} + V_{cn} = 0 . \quad (15)$$

The relationship between the converter output voltages V_{kn} (k = a, b, c) and the voltage V_{nO} is:

$$V_{kn} = V_{kO} - V_{nO} , \quad (16)$$

where $V_{nO} = (V_{aO} + V_{bO} + V_{cO}) / 3$.

Starting from (16), we express V_{an}, V_{bn} and V_{cn} in terms of V_{aO}, V_{bO} and V_{cO}:

$$V_{an} = (2/3)\cdot V_{aO} - (1/3)\cdot V_{bO} - (1/3)\cdot V_{cO} ; \quad (17)$$

$$V_{bn} = -(1/3)\cdot V_{aO} + (2/3)\cdot V_{bO} - (1/3)\cdot V_{cO} ; \quad (18)$$

$$V_{cn} = -(1/3)\cdot V_{aO} - (1/3)\cdot V_{bO} + (2/3)\cdot V_{cO} , \quad (19)$$

where V_{aO}, V_{bO}, V_{cO} are determined by (11).

STATCOM control strategy. The block diagram of the control strategy is shown in Fig. 3. This diagram consists of a dual-loop control structure: an inner current control loop and an outer current reference generation loop. In the outer loop, the DC voltage control loop is designed to maintain the DC-link voltage at its reference value.

The measured DC voltage is compared with the reference value, and the resulting error is processed by a PI controller. This controller generates the active current reference component I_{dref}, as shown in Fig. 3. Similarly, in the AC voltage regulation loop, the RMS value of the AC voltage measured at PCC is compared with a predefined reference voltage. The resulting error is processed by another PI controller, in which the proportional term provides a fast dynamic response to voltage variations,

while the integral term eliminates the steady-state error. The control signal produced by the controller is then converted into reactive current references I_{qref}, enabling the adjustment of the reactive power exchanged by the STATCOM, thereby ensuring effective voltage regulation at the PCC and enhancing the overall stability of the power system [7, 22]. The quantity V_{rms} denotes the measured value of the AC voltage, calculated from the components d and q of the 3-phase voltage vector:

$$V_{rms} = \sqrt{V_d^2 + V_q^2}\,. \tag{20}$$

The inner current control loop, implementing either SMC or the backstepping approach, subsequently computes the converter reference output voltages required for the modulation process.

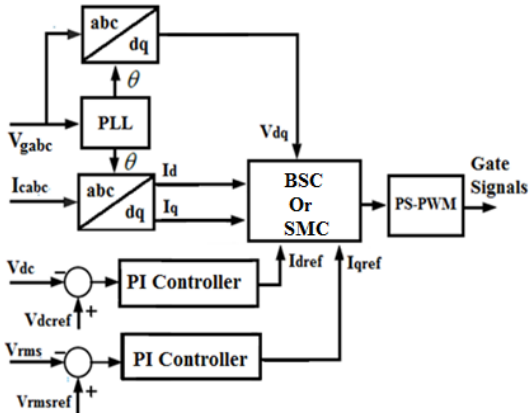

Fig. 3. STATCOM control block diagram

Sliding mode controller. In the control strategy, STATCOM is driven using SMC to regulate the STATCOM currents (I_d and I_q) [30, 31]. The equations of state (5) and (6) are expressed as follows:

$$\frac{\mathrm{d}I_d}{\mathrm{d}t} = -\frac{R}{L}I_d - \frac{1}{L}V_{cd} + \omega I_q + \frac{1}{L}V_d\,; \tag{21}$$

$$\frac{\mathrm{d}I_q}{\mathrm{d}t} = -\frac{R}{L}I_q - \frac{1}{L}V_{cq} - \omega I_d + \frac{1}{L}V_q\,, \tag{22}$$

with:

$$V_d = V_{d\_eq} + V_{dcr}\,; \tag{23}$$

$$V_q = V_{q\_eq} + V_{qcr}\,. \tag{24}$$

The implementation of SMC is initiated by the selection of sliding surfaces:

$$S_d = I_{dref} - I_d\,; \tag{25}$$

$$S_q = I_{qref} - I_q\,. \tag{26}$$

After derivation, we obtain:

$$\dot{S}_d = \dot{I}_{dref} - \dot{I}_d\,; \tag{27}$$

$$\dot{S}_q = \dot{I}_{qref} - \dot{I}_q\,. \tag{28}$$

Then, by substituting (21) into (27) and (22) into (28), we obtain:

$$\dot{S}_d = \dot{I}_{dref} - \dot{I}_d = \dot{I}_{dref} + \frac{R}{L}I_d - \omega I_q + \frac{1}{L}V_{cd} - \frac{1}{L}V_d\,; \tag{29}$$

$$\dot{S}_q = \dot{I}_{qref} - \dot{I}_q = \dot{I}_{qref} + \frac{R}{L}I_q + \omega I_d + \frac{1}{L}V_{cq} - \frac{1}{L}V_q\,. \tag{30}$$

And to check Lyapunov stability criterion $\dot{S}_i \times S_i < 0$ we must have:

$$\dot{S}_d = -k_d \cdot \mathrm{sign}(S_d)\,; \tag{31}$$

$$\dot{S}_q = -k_q \cdot \mathrm{sign}(S_q)\,, \tag{32}$$

where k_d, k_q are the design parameters chosen according to the desired performance in closed loop.

By substituting $\dot{S}_d$ and $\dot{S}_q$ with their expressions from (29), (30) into (31), (32), respectively, we obtain:

$$\dot{I}_{dref} + \frac{R}{L}I_d - \omega I_q + \frac{1}{L}V_{cd} - \frac{1}{L}V_d = -k_d \cdot \mathrm{sign}(S_d)\,, \tag{33}$$

$$\dot{I}_{qref} + \frac{R}{L}I_q + \omega I_d + \frac{1}{L}V_{cq} - \frac{1}{L}V_q = -k_q \cdot \mathrm{sign}(S_q)\,. \tag{34}$$

Consequently, the V_d and V_q control commands can be expressed as follows:

$$V_d = L\dot{I}_{dref} + RI_d - \omega L I_q + V_{cd} + L \cdot k_d \cdot \mathrm{sign}(S_d) = \\ = V_{d\_eq} + V_{dcr}\,; \tag{35}$$

$$V_q = L\dot{I}_{qref} + RI_q + \omega L I_d + V_{cq} + L \cdot k_q \cdot \mathrm{sign}(S_q) = \\ = V_{q\_eq} + V_{qcr}\,. \tag{36}$$

The following control and correction terms are obtained:

- equivalent commands terms:

$$V_{d\_eq} = L\dot{I}_{dref} + RI_d - \omega L I_q + V_{cd}\,; \tag{37}$$

$$V_{q\_eq} = L\dot{I}_{qref} + RI_q + \omega L I_d + V_{cq}\,; \tag{38}$$

- correction terms:

$$V_{dcr} = L \cdot k_d \cdot \mathrm{sign}(S_d)\,; \tag{39}$$

$$V_{qcr} = L \cdot k_q \cdot \mathrm{sign}(S_q)\,. \tag{40}$$

In MATLAB/Simulink implementation, the chattering phenomenon was alleviated by replacing the discontinuous sign(S) function with a Saturation block. This adjustment results in a smoother control behavior near the sliding surface while retaining the robustness and stability of the sliding mode controller.

Backstepping current controller. The backstepping approach is a robust nonlinear control strategy based on Lyapunov's stability theory, which enables a systematic linearization of nonlinear systems. The method consists in progressively constructing the control law by defining some state variables as virtual control inputs and designing intermediate control laws for each stage [32, 33]. The purpose of the BSC applied to the active and reactive currents is to guarantee that the active and reactive current components (I_d and I_q), accurately track their respective reference values I_{dref} and I_{qref}.

The tracking errors of these currents are defined by:

$$z_1 = I_{dref} - I_d\,; \tag{41}$$

$$z_2 = I_{qref} - I_q\,. \tag{42}$$

Their derivatives are given by:

$$\dot{z}_1 = \dot{I}_{dref} - \dot{I}_d\,; \tag{43}$$

$$\dot{z}_2 = \dot{I}_{qref} - \dot{I}_q\,. \tag{44}$$

Substituting (21) into (43) and (22) into (44), we obtain:

$$\dot{z}_1 = \dot{I}_{dref} + \frac{R}{L}I_d - \omega I_q - \frac{V_d - V_{cd}}{L}\,; \tag{45}$$

$$\dot{z}_2 = \dot{I}_{qref} + \frac{R}{L}I_q + \omega I_d - \frac{V_q - V_{cq}}{L}\,. \tag{46}$$

Lyapunov candidate functions are defined by:

$$V_1 = \frac{1}{2} z_1^2 ; \quad (47)$$

$$V_2 = \frac{1}{2} z_2^2 . \quad (48)$$

The derivation of these functions leads to:

$$\dot{V}_1 = z_1 \dot{z}_1 = z_1 \left(\dot{I}_{dref} + \frac{R}{L} I_d - \omega I_q - \frac{V_d - V_{cd}}{L} \right); \quad (49)$$

$$\dot{V}_2 = z_2 \dot{z}_2 = z_2 \left(\dot{I}_{qref} + \frac{R}{L} I_q + \omega I_d - \frac{V_q - V_{cq}}{L} \right). \quad (50)$$

To ensure the stability of the Lyapunov function, its derivative must always be negative. To achieve this, we choose:

$$\dot{z}_1 = -k_1 z_1 ; \quad (51)$$

$$\dot{z}_2 = -k_2 z_2 . \quad (52)$$

Replacing the expression for $\dot{z}_1$ in (45) and the expression for $\dot{z}_2$ in (46), we obtain:

$$\dot{I}_{dref} + \frac{R}{L} I_d - \omega I_q - \frac{V_d - V_{cd}}{L} = -k_1 z_1 ; \quad (53)$$

$$\dot{I}_{qref} + \frac{R}{L} I_q + \omega I_d - \frac{V_q - V_{cq}}{L} = -k_2 z_2 . \quad (54)$$

The commands V_{cd} and V_{cq} can then be defined by:

$$V_{cd} = L \left(-k_1 z_1 - \dot{I}_{dref} - \frac{R}{L} I_d + \omega I_q \right) + V_d ; \quad (55)$$

$$V_{cq} = L \left(-k_2 z_2 - \dot{I}_{qref} - \frac{R}{L} I_q - \omega I_d \right) + V_q , \quad (56)$$

where k_1 and k_2 are the positive constants.

The reference voltages in the dq frame, obtained from the output of the inner current control loop (whether based on SMC or the backstepping method), are transformed into the stationary (a, b, c) reference frame. These voltages are then compared with triangular carrier signals to generate the corresponding switching signals for the power switches. Several capacitor voltage balancing techniques have been proposed in the literature. Among these methods, the PS-PWM technique stands out for its ease of implementation and its superior performance in terms of total harmonic distortion (THD) compared to other techniques. It is based on the use of multiple triangular carrier signals with identical peak-to-peak amplitude and frequency, each phase-shifted relative to the previous one, with the phase shift expressed as $\varphi = 360°/p$ [34, 35].

Figure 4 shows the reference and carrier signals used in conventional PS-PWM modulation for a 4-cell, 5-level FCMC. In this topology, the PS-PWM method employs 4 carrier signals of identical amplitude and frequency, each phase-shifted by 90° relative to the preceding one (Fig. 5). A sinusoidal reference signal, varying within the interval [–1, 1] in the linear modulation region, is compared with all 4 carriers to generate the switching control signals. Each comparison generates a binary output: 1 if the reference signal is greater than or equal to the carrier, and 0 otherwise (Fig. 4).

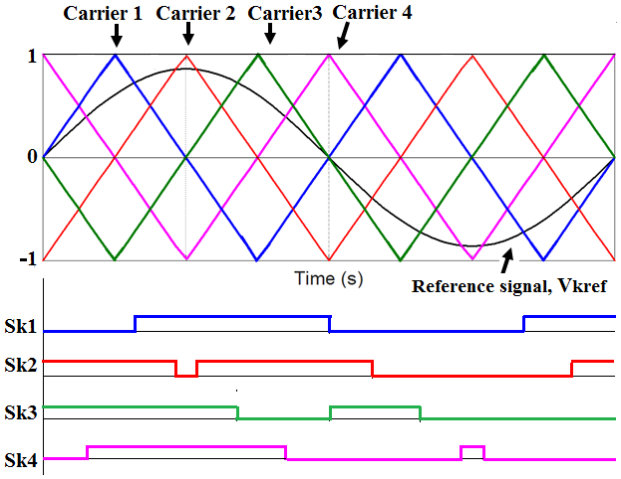

Fig. 4. PS-PWM technique for the 5-level FCMC

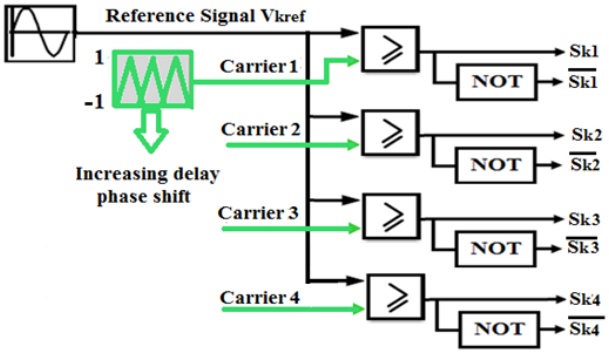

Fig. 5. Schematic diagram of the PS-PWM control

Simulation results and analysis. The complete electrical system, shown in Fig. 1, along with the proposed control strategy, illustrated in Fig. 3, was simulated in MATLAB/Simulink (SimPowerSystems) with a reactive power compensation capacity of ±100 kVAr, under various reactive load conditions, based on the main parameters summarized in Table 3. In the simulation scenario, load L1 is applied continuously from 0 to 8 s. At t = 0.4 s, an inductive load L2 is added, and at t = 0.6 s, a capacitive load L3 is applied while L2 is disconnected.

Table 3

Parameters of simulated system [36]

Component	Parameters	Value
AC source	Line-to-line RMS voltage	381 V
	Frequency	50 Hz
	Source resistance	7 mΩ
	Source inductance	0.23 mH
STATCOM	DC-link voltage	750 V
	L filter inductance	0.7 mH
Load	Fixed load L1	100 kW
	Dynamic load L2	10 kW / +50 kVAr
	load L3	10 kW / –50 kVAr

Figure 6 shows the effective per-phase voltage at the PCC, with and without STATCOM compensation, during the connection of reactive loads (inductive and capacitive). The red curve represents the PCC voltage without STATCOM operation. As observed, the voltage amplitude increases relative to the desired value between 0.2 s and 0.4 s due to the connection of capacitive loads, which inject additional reactive power into the network, causing an overvoltage. It then decreases between 0.4 s and 0.6 s relative to the nominal voltage due to the connection of

inductive loads, which absorb more reactive power, resulting in voltage sag. Conversely, the green curve illustrates the PCC voltage with the STATCOM operating under SMC. It is clearly observed that the voltage is accurately maintained at its reference value, exhibiting a very fast response time of approximately 1 ms, even during the connection of reactive loads. The blue curve shows the PCC voltage with the STATCOM controlled using the backstepping method, demonstrating its effectiveness in maintaining the voltage at the desired value, with a very fast response time and fewer fluctuations compared to the STATCOM under SMC.

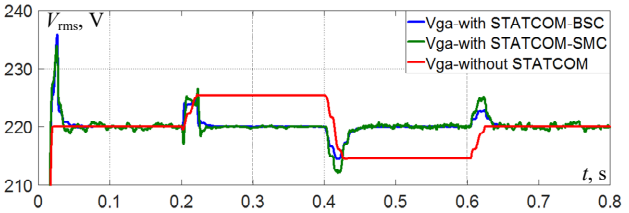

Fig. 6. RMS phase voltage at PCC without and with STATCOM

Figure 7 shows the 3-phase voltages at the PCC without the STATCOM during the connection of reactive loads. Overvoltages caused by capacitive loads can be observed between 0.2 s and 0.4 s, and voltage sags resulting from inductive loads appear between 0.4 s and 0.6 s.

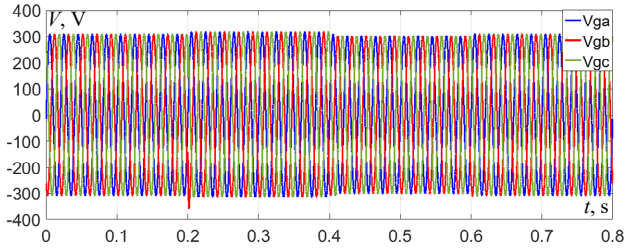

Fig. 7. 3-phase voltage (abc) at PCC without STATCOM

Figure 8 illustrates the 3-phase voltages at the PCC under STATCOM operation. The voltage waveforms clearly reach the desired values, demonstrating the responsiveness and effectiveness of the proposed controllers.

Figure 9 presents the dynamic response of the reactive power exchanged between the compensator and the AC network for the 2 proposed structures (SMC STATCOM and BSC STATCOM). It is clearly observed that both structures respond effectively to voltage disturbances caused by reactive loads at the PCC through the injection and absorption of reactive power. This figure confirms that the network remains in a steady state during the periods from 0 s to 0.2 s and from 0.6 s to 0.8 s, during which no reactive power is exchanged between the STATCOM and the network. In the interval 0.2 s to 0.4 s, the network experiences a voltage increase due to the connection of the capacitive load, and the STATCOM intervenes by absorbing the necessary reactive power to compensate for the excess, meaning that the STATCOM operates in inductive mode. In the interval from 0.4 s to 0.6 s, the network experiences voltage sag due to the connection of the inductive load, and the STATCOM intervenes by injecting the necessary reactive power to compensate for the loss, meaning that the STATCOM operates in capacitive mode.

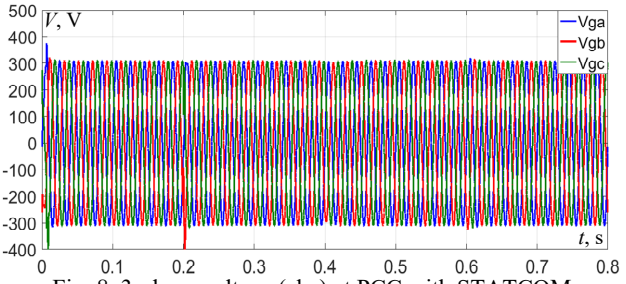

Fig. 8. 3-phase voltage (abc) at PCC with STATCOM

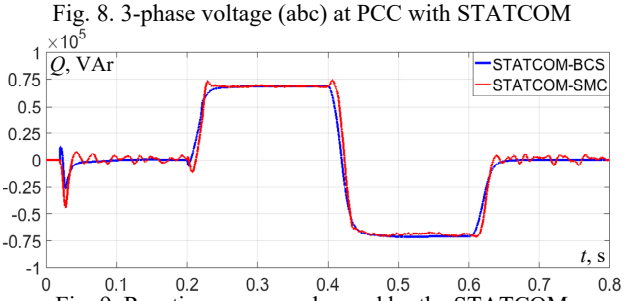

Fig. 9. Reactive power exchanged by the STATCOM

In Fig. 10, the phase voltage at the PCC and the phase current of the STATCOM compensator are shown. As observed, during the intervals from 0 to 0.2 s and from 0.6 s to 0.8 s, no disturbances affect the source, and no reactive power is supplied or absorbed by the compensator, resulting in zero current. Conversely, during the interval from 0.2 s to 0.3 s, the compensator operates in inductive mode: the STATCOM current lags the voltage by 90°. Finally, during the interval from 0.3 s to 0.4 s, the compensator operates in capacitive mode: the STATCOM current leads the voltage by 90°.

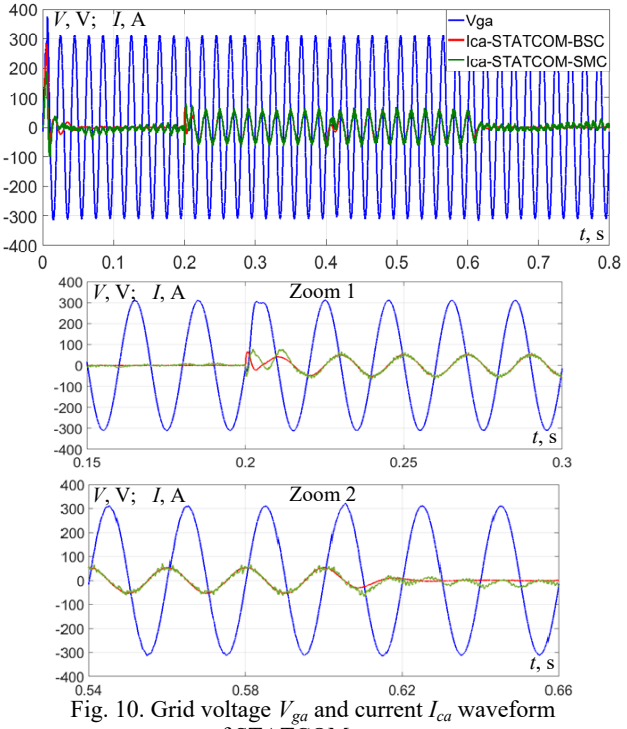

Fig. 10. Grid voltage V_{ga} and current I_{ca} waveform of STATCOM output

Figure 11 shows the evolution of the STATCOM DC bus voltage. This voltage stabilizes around 750 V, with minor fluctuations not exceeding 4 % for both structures (SMC STATCOM and BSC STATCOM) during the voltage sag and overvoltage intervals caused by reactive loads. It is also observed that the fluctuations are slightly smaller for the SMC STATCOM compared to the BSC STATCOM.

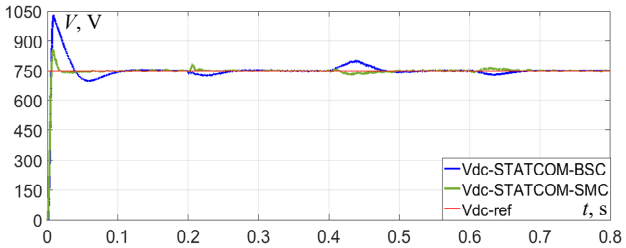

Fig. 11. STATCOM DC voltage response

Figure 12 shows the network phase voltage (V_{ga}) and the corresponding phase current (I_{ga}) at the PCC in the absence of the STATCOM. It can be observed that the current leads the source voltage (capacitive behavior) during the interval 0.2 s to 0.4 s, and lags behind it (inductive behavior) during the interval 0.4 s to 0.6 s. These phase shifts between the network voltage and current, caused by the presence of capacitive and inductive loads, disturb the stability of reactive power and deteriorate the power quality within the electrical system.

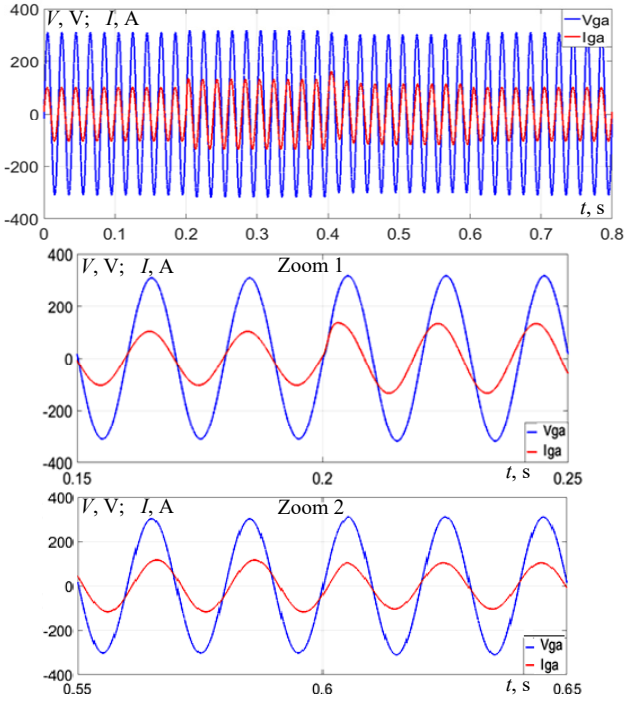

Fig. 12. Grid voltage V_{ga} and current I_{ga} without STATCOM

Figure 13 shows the voltage and current waveforms of phase A at the point of PCC during STATCOM operation. It can be observed that the current and voltage are nearly in phase, with the STATCOM effectively compensating the reactive power supplied by the capacitive loads between 0.2 s and 0.4 s, and the reactive power absorbed by the inductive loads between 0.4 s and 0.6 s, thereby achieving a unity power factor. These results confirm the STATCOM's capability to maintain a sinusoidal current aligned with the grid voltage at the PCC, irrespective of load variations.

Figures 14, 15 show the voltage between phase A and the neutral point O (V_{caO}) at the converter output for both STATCOM-BSC and STATCOM-SMC structures. It is clearly observed that this voltage exhibits 5 distinct and symmetrical levels: $\pm V_{dc}/2$, $\pm V_{dc}/4$ and 0.

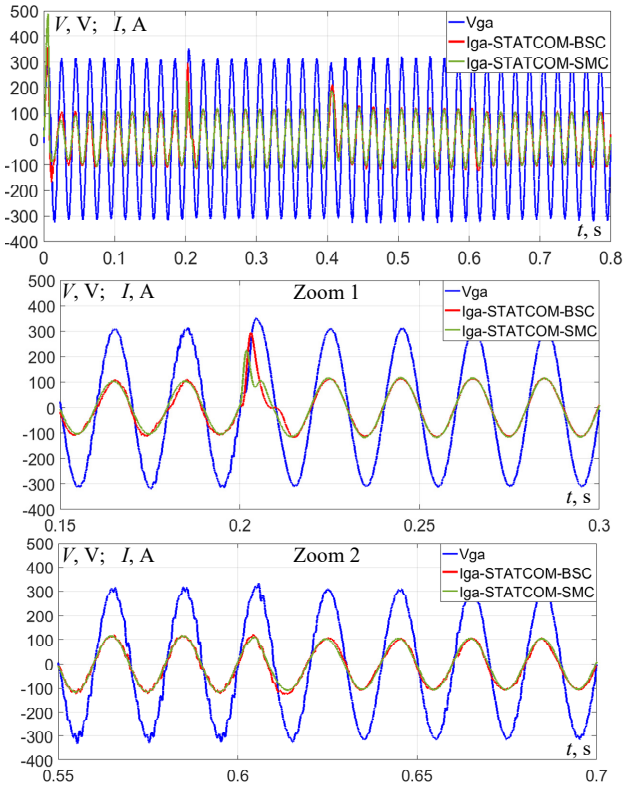

Fig. 13. Grid voltage V_{ga} and current I_{ga} with STATCOM

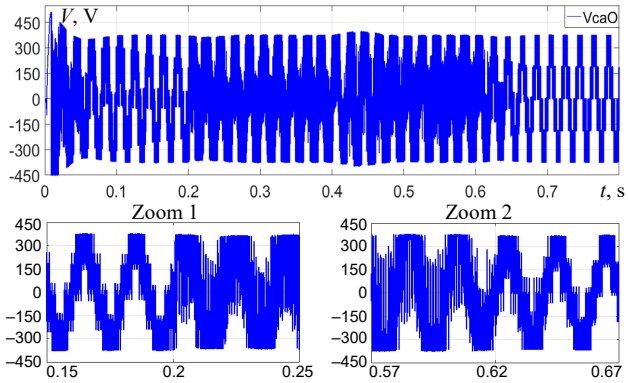

Fig. 14. Output phase voltage V_{caO} of the STATCOM-BSC converter

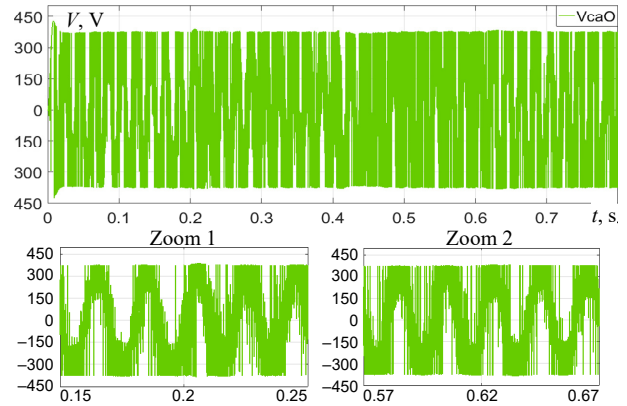

Fig. 15. Output phase voltage V_{caO} of the STATCOM-SMC converter

Figures 16, 17 illustrate the line-to-line voltage (V_{cab}) between phases A and B at the converter output for the same structures, in which the voltage displays 9 levels: $-V_{dc}$; $-3V_{dc}/4$; $-V_{dc}/2$; $-V_{dc}/4$; 0; $V_{dc}/4$; $V_{dc}/2$; $3V_{dc}/4$; V_{dc} thereby confirming the proper operation of the multilevel converter and the accuracy of the applied modulation.

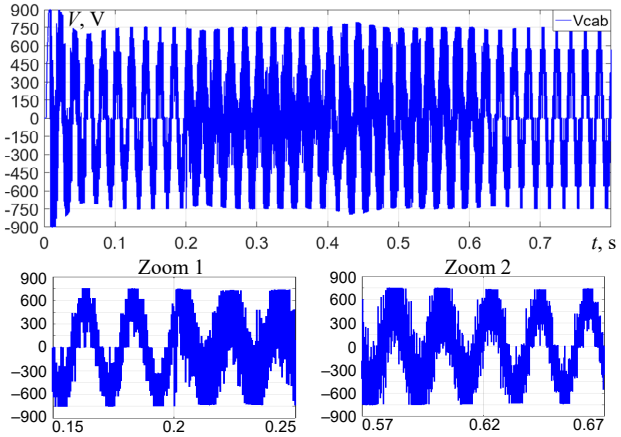

Fig. 16. Line-to-line output voltage V_{cab} of the STATCOM-BSC converter

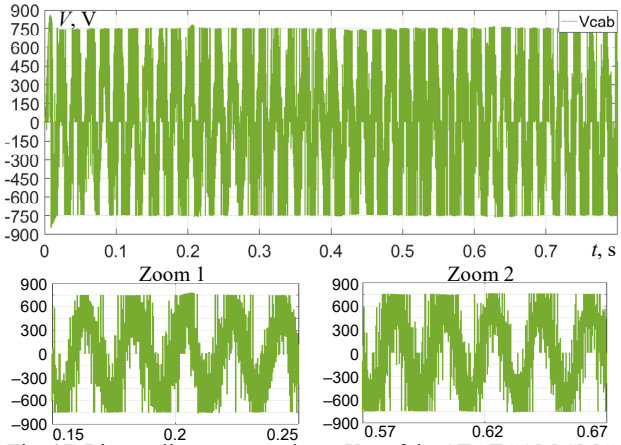

Fig. 17. Line-to-line output voltage V_{cab} of the STATCOM-SMC converter

Figure 18 illustrates the evolution of the internal flying capacitor voltages of the converter for phase of the STATCOM during the connection of reactive loads. A natural balancing of the flying capacitor voltages is also observed, achieved through the PS-PWM control technique. The voltage variations of the capacitors become more pronounced during the time interval between 0.2 s and 0.6 s, due to the reactive power supplied to or absorbed by the reactive loads.

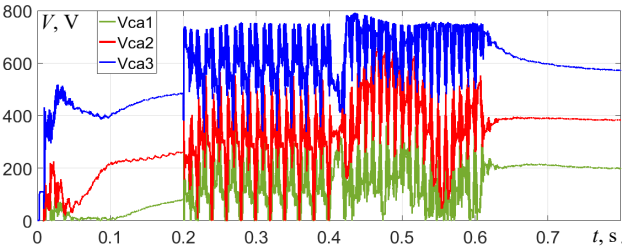

Fig. 18. Voltages of the flying capacitors in the FCMC

A harmonic analysis of the phase voltage V_{sa} at the PCC was performed using the FFT (fast Fourier transform) block in MATLAB for the two STATCOM structures, controlled respectively by SMC and BSC, under voltage sags and swells caused by reactive loads. As shown in Table 4, both structures exhibit almost identical fundamental voltage values. However, the backstepping mode-controlled STATCOM demonstrates better performance in terms of THD. Nevertheless, the THD values for both structures remain within the limits of the IEEE Std. 519-1992.

Table 4

Comparison of performance of SMC and BSC

	THD of V_{sa} at PCC, %	Fundamental V_{sa} at PCC, V
STATCOM SMC	3.13	310.1
STATCOM BSC	4.44	310

Conclusions. This paper presented a comparative analysis of the performance of two nonlinear control strategies, namely backstepping and sliding mode, applied to a STATCOM based on a 5-level series multicell flying-capacitor converter, for dynamic reactive power compensation, voltage regulation, and power factor improvement in a low-voltage network. The control strategies were implemented to ensure accurate tracking of active and reactive currents as well as stable voltage regulation. The study showed that the connection or disconnection of inductive and capacitive loads, causing voltage sags or swells, can be effectively compensated by the STATCOM.

The STATCOM model and the two control strategies were implemented in MATLAB/Simulink. The simulation results demonstrated that both controllers can maintain a stable voltage at the PCC with a fast dynamic response of approximately 1 ms, due to the almost instantaneous injection or absorption of reactive power, even under network disturbances such as load variations, voltage sags, and swells. In addition, the THD of the PCC voltage remains well below the 5 % limit specified by the IEEE-519 standard, with values of 3.13 % for BSC and 4.44 % for SMC, showing that the BSC strategy achieves superior harmonic performance.

Future works should focus on experimental validation of these control strategies under real operating conditions, as well as on further optimization of dynamic performance and capacitor-voltage balancing.

Conflict of interest. The authors declare that they have no conflicts of interest.

REFERENCES

1. Asoodar M., Nahalparvari M., Zhang Y., Danielsson C., Nee H.-P., Blaabjerg F. Accurate Condition Monitoring of Semiconductor Devices in Cascaded H-Bridge Modular Multilevel Converters. *IEEE Transactions on Power Electronics*, 2023, vol. 38, no. 3, pp. 3870-3884. doi: https://doi.org/10.1109/TPEL.2022.3221285.

2. Carbonara A., Dambone Sessa S., L'Abbate A., Sanniti F., Chiumeo R. Comparison of Advanced Flexible Alternating Current Transmission System (FACTS) Devices with Conventional Technologies for Power System Stability Enhancement: An Updated Review. *Electronics*, 2024, vol. 13, no. 21, art. no. 4262. doi: https://doi.org/10.3390/electronics13214262.

3. Pires V.F., Cordeiro A., Foito D., Silva J.F. A Multilevel Converter Topology for a STATCOM System Based on Four-Leg Two-Level Inverters and Cascaded Scott Transformers. *IEEE Transactions on Power Delivery*, 2022, vol. 37, no. 3, pp. 1391-1402. doi: https://doi.org/10.1109/TPWRD.2021.3086399.

4. Sharma S., Gupta S., Zuhaib M., Bhuria V., Malik H., Almutairi A., Afthanorhan A., Hossaini M.A. A Comprehensive Review on STATCOM: Paradigm of Modeling, Control, Stability, Optimal Location, Integration, Application, and Installation. *IEEE Access*, 2024, vol. 12, pp. 2701-2729. doi: https://doi.org/10.1109/ACCESS.2023.3345216.

5. He C., Yang B., Luo Z., Liu G. Research on a New Topology and Reactive Power Compensation Application of Reinjection Multilevel Voltage Source Converter. *Applied Sciences*, 2024, vol. 14, no. 21, art. no. 9998. doi: https://doi.org/10.3390/app14219998.

6. Sharma H., Nanda H., Yadav A. Novel nine level switched capacitor multi-level inverter based STATCOM for distribution system. *Computers and Electrical Engineering*, 2024, vol. 120, art. no. 109647. doi: https://doi.org/10.1016/j.compeleceng.2024.109647.

7. Atanalian S., Sebaaly F., Zgheib R., Al-Haddad K. Z Packed U-Cell Modular Multilevel Converter for STATCOM Applications. *IEEE*

Access, 2025, vol. 13, pp. 78795-78807. doi: https://doi.org/10.1109/ACCESS.2025.3566015.
8. Heidari M., Kovsarian A., Seifossadat S.Gh. Power quality improvement with cascaded multilevel converter based STATCOM. *IIUM Engineering Journal*, 2018, vol. 19, no. 1, pp. 91-103. doi: https://doi.org/10.31436/iiumej.v19i1.873.
9. Hassan R.F., Shyaa S.S. Design and Analysis of the STATCOM Based on Diode Clamped Multilevel Converter Using Model Predictive Current Control Strategy. *European Journal of Electrical Engineering*, 2021, vol. 23, no. 3, pp. 221-228. doi: https://doi.org/10.18280/ejee.230306.
10. Neyshabouri Y., Chaudhary S.K., Teodorescu R., Sajadi R., Iman-Eini H. Improving the Reactive Current Compensation Capability of Cascaded H-Bridge Based STATCOM Under Unbalanced Grid Voltage. *IEEE Journal of Emerging and Selected Topics in Power Electronics*, 2020, vol. 8, no. 2, pp. 1466-1476. doi: https://doi.org/10.1109/JESTPE.2019.2916571.
11. Hasanzadeh S., Shojaeian H., Mohsenzadeh M.M., Heydarian-Forushani E., Alhelou H.H., Siano P. Power Quality Enhancement of the Distribution Network by Multilevel STATCOM-Compensated Based on Improved One-Cycle Controller. *IEEE Access*, 2022, vol. 10, pp. 50578-50588. doi: https://doi.org/10.1109/ACCESS.2022.3172144.
12. Cheng Q., Wang C., Chen Z. A Dual Modulation Waveform PWM Combined With Phase-Shifted Carriers in Stacked Multicell Converter. *IEEE Transactions on Power Electronics*, 2021, vol. 36, no. 12, pp. 14456-14465. doi: https://doi.org/10.1109/TPEL.2021.3088463.
13. Tebaldi D. An Approach to Control Multilevel Flying-Capacitor Converters Using Optimal Dynamic Programming Benchmark. *Electronics*, 2025, vol. 14, no. 5, art. no. 948. doi: https://doi.org/10.3390/electronics14050948.
14. Mersche S.C., Schwendemann R., Hiller M. Validation of the Quasi-Two-Level Operation for a Flying Capacitor Converter in Medium-Voltage Applications. *Energies*, 2023, vol. 16, no. 6, art. no. 2797. doi: https://doi.org/10.3390/en16062797.
15. Ebrahimi J., Esfahani F.N., Eren S., Bakhshai A. An Active Capacitor Voltage Balancing Method for a Four-Level Single Flying Capacitor Converter. *IECON 2024 - 50th Annual Conference of the IEEE Industrial Electronics Society*, 2024, pp. 1-6. doi: https://doi.org/10.1109/IECON55916.2024.10905229.
16. Laamiri S., Ghanes M., Santomenna G. Observer based direct control strategy for a multi-level three phase flying-capacitor inverter. *Control Engineering Practice*, 2019, vol. 86, pp. 155-165. doi: https://doi.org/10.1016/j.conengprac.2019.03.011.
17. Redouane A., Saou R., Oukaour A. Flying Capacitor Voltage Balancing Control Strategy Based on Logic-equations in Five Level ANPC Inverter. *Periodica Polytechnica Electrical Engineering and Computer Science*, 2023, vol. 67, no. 4, pp. 438-448. doi: https://doi.org/10.3311/PPee.21879.
18. Buso S., Rossetto L. Damping of Flying Capacitor Dynamics in Multi-Level Boost DC-DC Converters. *Electronics*, 2024, vol. 13, no. 24, art. no. 4883. doi: https://doi.org/10.3390/electronics13244883.
19. Ramakrishna E., Gadhamappagari J., Sujatha P. Auto tuning of PI Gains using Cuttlefish Optimization for DC Link Voltage Control in a 5-level HB MMC D-STATCOM. *Engineering, Technology & Applied Science Research*, 2023, vol. 13, no. 6, pp. 12086-12091. doi: https://doi.org/10.48084/etasr.6413.
20. Stepanov A., Saad H., Mahseredjian J. Modeling of MMC-based STATCOM with embedded energy storage for the simulation of electromagnetic transients. *Electric Power Systems Research*, 2023, vol. 220, art. no. 109316. doi: https://doi.org/10.1016/j.epsr.2023.109316.
21. Yu L., Wang G., Wu T., Zhu J., Booth C.D. Variable DC voltage based reactive power enhancement scheme for MMC-STATCOM. *IET Smart Grid*, 2024, vol. 7, no. 4, pp. 427-441. doi: https://doi.org/10.1049/stg2.12147.
22. Ahmed T., Waqar A., Elavarasan R.M., Imtiaz J., Premkumar M., Subramaniam U. Analysis of Fractional Order Sliding Mode Control in a D-STATCOM Integrated Power Distribution System. *IEEE Access*, 2021, vol. 9, pp. 70337-70352. doi: https://doi.org/10.1109/ACCESS.2021.3078608.
23. Boghdady T.A., Mohamed Y.A. Reactive power compensation using STATCOM in a PV grid connected system with a modified MPPT method. *Ain Shams Engineering Journal*, 2023, vol. 14, no. 8, art. no. 102060. doi: https://doi.org/10.1016/j.asej.2022.102060.
24. Freire D.F.M., Caseiro L.M.A., Mendes A.M.S. Model Predictive Control of a five-level Neutral-Point-Clamped STATCOM. *2019 IEEE International Conference on Industrial Technology (ICIT)*, 2019, pp. 1482-1487. doi: https://doi.org/10.1109/ICIT.2019.8755208.
25. Jin Y., Xiao Q., Jia H., Mu Y., Ji Y., Teodorescu R., Dragicevic T. A Dual-Layer Back-Stepping Control Method for Lyapunov Stability in Modular Multilevel Converter Based STATCOM. *IEEE Transactions on Industrial Electronics*, 2022, vol. 69, no. 3, pp. 2166-2179. doi: https://doi.org/10.1109/TIE.2021.3063973.
26. Djellad A., Belakehal S., Chenni R., Dekhane A. Reliability Improvement in Serial Multicellular Converters Based on STATCOM Control. *Journal Europeen des Systemes Automatises*, 2021, vol. 54, no. 4, pp. 519-528. doi: https://doi.org/10.18280/jesa.540401.
27. Bressan M.V., Rech C., Batschauer A.L. Design of flying capacitors for n-level FC and n-level SMC. *International Journal of Electrical Power & Energy Systems*, 2019, vol. 113, pp. 220-228. doi: https://doi.org/10.1016/j.ijepes.2019.05.030.
28. El Khlifi Y., El Magri A., Lajouad R., Bouattane O., Giri F. Output-feedback control of a grid-connected photovoltaic system based on a multilevel flying-capacitor inverter with power smoothing capability. *ISA Transactions*, 2024, vol. 147, pp. 360-381. doi: https://doi.org/10.1016/j.isatra.2024.02.007.
29. El Khlif Y., El Magri A., Lajouad R., Bouattane O. Hybrid feedback control of PMSG-based WECS with multilevel flying-capacitor inverter enhanced by fractional order extremum seeking. *E-Prime - Advances in Electrical Engineering, Electronics and Energy*, 2024, vol. 10, art. no. 100760. doi: https://doi.org/10.1016/j.prime.2024.100760.
30. Kerrouche K.D.E., Lodhi E., Kerrouche M.B., Wang L., Zhu F., Xiong G. Modeling and design of the improved D-STATCOM control for power distribution grid. *SN Applied Sciences*, 2020, vol. 2, no. 9, art. no. 1519. doi: https://doi.org/10.1007/s42452-020-03315-8.
31. Belila H., Boudjerda N., Boubakir A., Bahri I. Improved STATCOM efficiency using a hybrid technique based on sliding mode control and proportional integral control. *Przegląd Elektrotechniczny*, 2020, vol. 96, no. 10, pp. 156-162. doi: https://doi.org/10.15199/48.2020.10.29.
32. Mazouz F., Belkacem S., Boukhalfa G., Colak I. Backstepping Approach Based on Direct Power Control of a DFIG in WECS. *2021 10th International Conference on Renewable Energy Research and Application (ICRERA)*, 2021, pp. 198-202. doi: https://doi.org/10.1109/ICRERA52334.2021.9598599.
33. El Ouanjli N., Derouich A., El Ghzizal A., Bouchnaif J., El Mourabit Y., Taoussi M., Bossoufi B. Real-time implementation in dSPACE of DTC-backstepping for a doubly fed induction motor. *The European Physical Journal Plus*, 2019, vol. 134, no. 11, art. no. 566. doi: https://doi.org/10.1140/epjp/i2019-12961-x.
34. Vijaya Sambhavi Y., Vijayapriya R. Phase disposition PWM control topology based: A novel multilevel inverter with reduced switch for power electronics applications. *Heliyon*, 2024, vol. 10, no. 21, art. no. e39856. doi: https://doi.org/10.1016/j.heliyon.2024.e39856.
35. Oghorada O.J.K., Zhang L., Esan B.A., Dickson E. Carrier-based sinusoidal pulse-width modulation techniques for flying capacitor modular multi-level cascaded converter. *Heliyon*, 2019, vol. 5, no. 12, art. no. e03022. doi: https://doi.org/10.1016/j.heliyon.2019.e03022.
36. Deniz E., Tuncer S., Gençoglu M.T. Voltage regulation in a distribution system by using STATCOM with three-level diode clamped inverter. *Proceedings of the 5th International Advanced Technologies Symposium*, 2009, pp. 1036-1042.

Received 24.10.2025
Accepted 28.11.2025
Published 02.03.2026

S. Belakehal [1]*, PhD, Associate Professor,*
M.L. Srief [1]*, PhD Student,*
[1] Laboratory of Electrical Engineering – Constantine LGEC, Department of Electrical Engineering,
Mentouri Brothers University, Constantine, 25000, Algeria,
e-mail: belakehal.soltane@umc.edu.dz (Corresponding Author); mohamedlaminesrief@gmail.com

How to cite this article:
Belakehal S., Srief M.L. Comparative performance analysis of backstepping and sliding mode control for static synchronous compensators based on flying capacitor multicell converters. *Electrical Engineering & Electromechanics*, 2026, no. 2, pp. 22-30. doi: https://doi.org/10.20998/2074-272X.2026.2.04